

# Star Formation Sequence in a Hierarchical Universe

ChangHoon Hahn<sup>1,2</sup>, Jeremy L. Tinker<sup>2</sup>, Andrew R. Wetzel<sup>3,4,5</sup>

changhoon.hahn@lbl.gov

DRAFT --- 136d026 --- 2018-08-16 --- NOT READY FOR DISTRIBUTION

## ABSTRACT

**motivation, methodology, impact.** In observations star forming galaxies form a tight  $\log M_*$  to  $\log SFR$  relation referred to as the *star formation main sequence* (SFS) out to  $z \sim 2$ . Beyond the evolution “along” this SFS, however, the star formation histories of star forming galaxies have not been precisely characterized. The SFH of these galaxies govern SMF, SFS, and also observed constraints on the stellar mass to halo mass relation.

By combining high-resolution cosmological  $N$ -body simulation with observed evolutionary trends of SF galaxies, we construct a model that tracks the evolution of star forming central galaxies over the redshift  $z < 1$ . Comparing this model

Observations find a remarkably small scatter in the stellar mass to halo mass relation. Somehow the star formation histories of galaxies must

According to observations, star forming galaxies form a tight  $\log M_*$  to  $\log SFR$  relation referred to as the “star formation main sequence” out to  $z \sim 2$ .

*Subject headings:* methods: numerical – galaxies: clusters: general – galaxies: groups: general – galaxies: evolution – galaxies: haloes – galaxies: star formation – cosmology: observations.

## 1. Introduction

- Motivate why we think SF galaxies evolve along the main sequence
- Discuss the current thought process on galaxy assembly bias
- Explain the limitation of SFH derivable from observations (Claire’s fisher matrix paper would be really good; ask her about the details)

---

<sup>1</sup>Lawrence Berkeley National Laboratory, 1 Cyclotron Road, Berkeley, CA 94720

<sup>2</sup>Center for Cosmology and Particle Physics, Department of Physics, New York University, 4 Washington Place, New York, NY 10003

<sup>3</sup>TAPIR, California Institute of Technology, Pasadena, CA USA

<sup>4</sup>Carnegie Observatories, Pasadena, CA USA

<sup>5</sup>Department of Physics, University of California, Davis, CA USA

- in fact we can’t constrain sf variability very well even in simulations due to the time resolution (see Hahn et al. (in prep.)).
- Observations also can’t provide detail host dark matter halo properties
- So the approach with combining observations with N-body (empirical modeling) is very effective in the context of the halo.
- Maybe talk about how the bigger context of why this is important?
- Why only centrals – because our current best understanding of satellites is that they quench after infall, so it doesn’t make sense to look at them
- our model goes from  $z < 1$  because beyond that the observations are statistically meaningless.

## 2. Central Galaxies of SDSS DR7

We construct our galaxy sample following the sample selection of [Tinker et al. \(2011\)](#). We select a volume-limited sample of galaxies with  $M_r 5\log(h) < 18$  and complete in  $M_* > 10^{9.4} M_\odot$  from the NYU Value-Added Galaxy Catalog (VAGC; [Blanton et al. 2005](#)) of the Sloan Digital Sky Survey Data Release 7 (SDSS DR7; [Abazajian et al. 2009](#)) at  $z \approx 0.04$ . The stellar masses of these galaxies are estimated using the `kcorrect` code ([Blanton & Roweis 2007](#)) assuming a [Chabrier \(2003\)](#) initial mass function. The star formation of the galaxies are estimated spectroscopically using the specific star formation rates (SSFR) from the current release of the MPA-JHU spectral reductions<sup>1</sup> ([Brinchmann et al. 2004](#)). Generally speaking,  $\text{SSFR} > 10^{-11} \text{yr}^{-1}$  are derived from  $\text{H}_\alpha$  emission,  $10^{-11} > \text{SSFR} > 10^{-12} \text{yr}^{-1}$  are derived from a combination of emission lines, and  $\text{SSFR} < 10^{-12} \text{yr}^{-1}$  are based on  $D_n4000$  (see discussion in [Wetzel et al. 2013](#)). We note that  $\text{SSFR} < 10^{-12} \text{yr}^{-1}$  should only be considered upper limits to the true galaxy SSFR ([Salim et al. 2007](#)).

From our galaxy sample, we identify the central galaxies using the [Tinker et al. \(2011\)](#) halo-based group-finding algorithm, which is based on the [Yang et al. \(2005\)](#) algorithm and tested in [Campbell et al. \(2015\)](#). The algorithm assigns a probability of being a satellite,  $P_{\text{sat}}$ , to each galaxy in the sample. Galaxies with  $P_{\text{sat}} \geq 0.5$  are classified as satellites and  $P_{\text{sat}} < 0.5$  are classified as centrals. In this paper we focus on central galaxies. With any group finding algorithm, galaxies are misassigned due to projection effects and redshift space distortions. The purity of the full central galaxy sample is  $\sim 90\%$  with a completeness of  $\sim 95\%$  ([Tinker et al. 2017](#)). Furthermore, [Campbell et al. \(2015\)](#) find that the algorithm

---

<sup>1</sup><http://wwwmpa.mpa-garching.mpg.de/SDSS/DR7/>

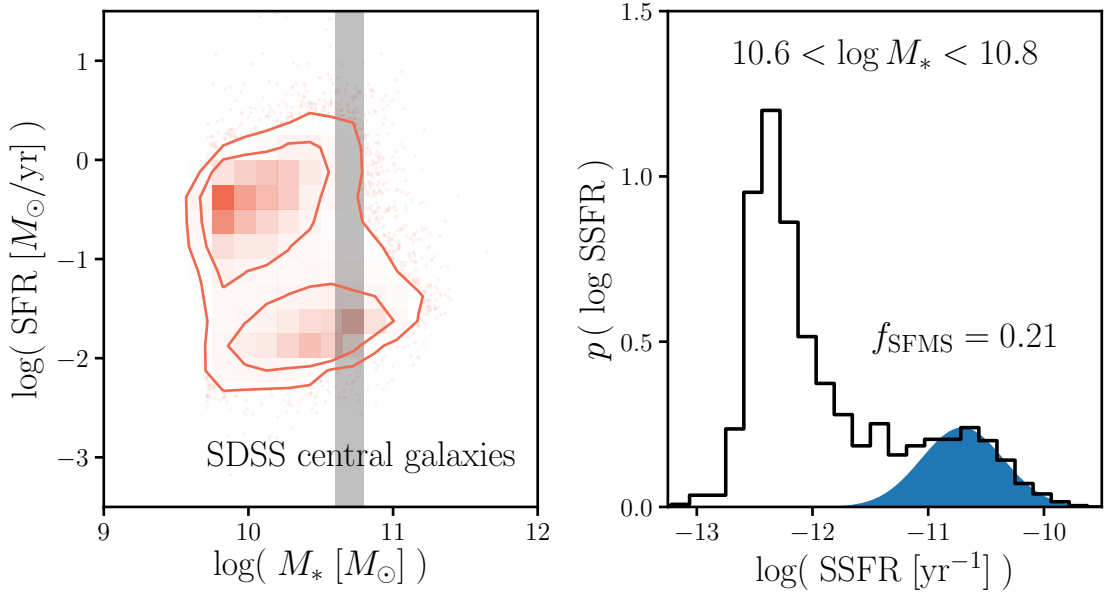


Fig. 1.— Central galaxies of the SDSS DR7 group catalog. *Left:* We plot the SFR- $M_*$  relation of the SDSS central galaxies. The contours illustrate the bimodal distribution of the galaxy properties and mark the star-forming and quiescent populations. The transitioning galaxies lie on the “green” valley between the star-forming and quiescent modes. *Right:* We plot the distribution of  $\log \text{SSFR}$  for SDSS centrals with  $10.6 < \log M_* < 10.8$ . Shaded in blue, we plot the SFS component of our GMM fit of the SFR- $M_*$  relation described in Section 3.1. Based on this fit, galaxies in the SFS account for approximately  $f_{\text{SFS}} = 0.21$  of the central galaxies in the stellar mass bin.

robustly identifies red and blue centrals as a function of stellar mass, which is highly relevant to our analysis.

In the left panel of Figure 1, we plot the SFR- $M_*$  distribution of the SDSS DR7 central galaxies. In the right panel, we plot the distribution of SSFR,  $p(\log \text{SSFR})$ , for galaxies with  $10.6 < \log M_* < 10.8$  (stellar mass range highlighted on the left panel). Both panels of Figure 1 illustrate the bimodality in the galaxy sample. The SFR- $M_*$  distribution also illustrates the correlation between SFR and  $M_*$  in star-forming galaxies *i.e.* the star-formation main sequence (SFS).

### 3. Model: Simulated Central Galaxies

We’re interesting in constructing a model that tracks central galaxies and their star formation within the heirarchical growth of their host halos. This requires a cosmological  $N$ -body simulation that accounts for the complex dynamical processes that govern the host halos of galaxies. In this paper we use the high resolution  $N$ -body simulation from Wetzel et al. (2013) generated using the White (2002) TreePM code with flat  $\Lambda$ CDM cosmology ( $\Omega_m = 0.274$ ,  $\Omega_b = 0.0457$ ,  $h = 0.7$ ,  $n = 0.95$ , and  $\sigma_8 = 0.8$ ). From initial conditions at  $z = 150$  generated from second-order Lagrangian Perturbation Theory,  $2048^3$  particles with mass of  $1.98 \times 10^8 M_\odot$  are evolved in a  $250\text{Mpc}/h$  box with a Plummer equivalent smoothing of  $2.5 \text{ kpc}/h$ . For a more detailed description of the simulation, we refer readers to Wetzel et al. (2013, 2014).

From the TreePM  $N$ -body simulation, ‘host halos’ are identified using the Friends-of-Friends (FoF) algorithm of Davis et al. (1985) with linking length of  $b = 0.168$  times the mean inter-particle spacing. Within these host halos, Wetzel et al. (2013) identifies ‘subhalos’ as overdensities in phase space through a six-dimensional FoF algorithm (FoF6D White et al. 2010). The host halos and subhalos are then tracked across the simulation outputs from  $z = 10$  to  $0$  to build merger trees (Wetzel et al. 2009; Wetzel & White 2010). The most massive subhalos in newly-formed host halos at a given simulation output are defined as the ‘central’ subhalo. A central subhalo retains its ‘central’ definition until it falls into a more massive host halo, at which point it becomes a ‘satellite’ subhalo.

At a given snapshot, we assign stellar masses used only for initializing our model to each subhalo by subhalo abundance matching (SHAM; Conroy et al. 2006; Vale & Ostriker 2006; Yang et al. 2009; Wetzel et al. 2012; Leja et al. 2013; Wetzel et al. 2013, 2014; ?) to  $M_{\text{peak}}$ , the maximum host halo mass that it ever had as a central subhalo. SHAM, in its simplest form, assumes a one-to-one mapping between subhalo  $M_{\text{peak}}$  and galaxy stellar mass  $M_*$  that preserves rank order:  $n(> M_{\text{peak}}) > n(> M_*)$ . In practice, we apply a 0.2 dex log-normal scatter in  $M$  at fixed  $M_{\text{peak}}$  based on the observed stellar to halo mass relation (SHMR; **bunch of SMHMR citations**). For  $n(> M_*)$ , we use observed stellar mass functions (SMFs) at the redshift corresponding to the snapshot. At  $z = 0.05$ , the lowest redshift

snapshot of our model, we use the SMF from [Li & White \(2009\)](#), which is based on the same SDSS NYU-VAGC sample as our group catalog. At higher redshifts, we interpolate between the [Li & White \(2009\)](#) SMF and the SMF from [Marchesini et al. \(2009\)](#) at  $z = 1.6$ . We choose the [Marchesini et al. \(2009\)](#) SMF, among others, because it produces interpolated SMFs that monotonically increase at  $z < 1$ . As noted in [?](#), at  $z \approx 1$ , the SMF interpolated between the [Li & White \(2009\)](#) and [Marchesini et al. \(2009\)](#) SMFs is consistent with more recent measurements from [Muzzin et al. \(2013\)](#) and [Ilbert et al. \(2013\)](#). **TBD: Perhaps mention in appendix how we test different SMF assumptions**

Throughout its 45 snapshot outs, **TreePM** simulation tracks the evolution of subhalos back to  $z \sim 10$ . We restrict ourselves to 15 snapshots from  $z = 1.08$  to  $z = 0.05$ , where we have the most statistically meaningful observations. Furthermore, since we’re interested in centrals we only keep subhalos that are classified as centrals throughout the redshift range. This criterion removes “black splash” or “ejected” satellite galaxies (*e.g.* [Mamon et al. 2004](#); [Wetzel et al. 2014](#)) misclassified as centrals. Finally, we have a model based on the **TreePM**  $N$ -body simulation that tracks the evolution of central subhalos from  $z = 1.08$  to  $z = 0.05$ . Next, we describe how we select and initialize the star forming central galaxies from the central subhalos in our model.

### 3.1. Selecting Star Forming Centrals

In our model, we’re interested in tracking the SFR and stellar mass evolution of SF central galaxies. To construct such a model, we first need to select SF galaxies from the central galaxies in our simulation, described above. Since we want our model to reproduce observations, our selection is based on  $f_{\text{SFS}}^{\text{cen}}(M_*)$ , the fraction of central galaxies within the star forming sequence, measured from the SDSS DR7 VAGC (Section 2). Below, we describe how we derive this  $f_{\text{SFS}}^{\text{cen}}(M_*)$  and use it to select SF central galaxies in our model. Afterwards we describe how we initialize the SFRs and  $M_*$  of these galaxies in our model.

Often in the literature, an empirical color-color or SFR– $M_*$  cut that separates the two main modes (red/blue or star-forming/quiescent) in the distribution is chosen to classify galaxies (*e.g.* [Baldry et al. 2006](#); [Blanton & Moustakas 2009](#); [Drory et al. 2009](#); [Peng et al. 2010](#); [Moustakas et al. 2013](#); [Hahn et al. 2015](#)). The red/quiescent or blue/star-forming fractions derived from this sort of classification, by construction, depend on the choice of cut and neglect galaxy subpopulations such as transitioning galaxies *i.e.* galaxies in the “green valley”. Instead, for our  $f_{\text{SFS}}^{\text{cen}}(M_*)$ , we use the SFS fitting method from [Hahn et al. \(in prep.\)](#). [Hahn et al. \(in prep.\)](#) uses Gaussian Mixture Models and the Bayesian Information Criteria in order to fit the SFR– $M_*$  relation of a galaxy population and identify its SFS. This data-driven approach relaxes many of the assumptions and hard cuts that go into other methods. Furthermore, as they demonstrate in [Hahn et al. \(in prep.\)](#) by applying to multiple simulations, it can be flexibly applied to a wide range of star formation and  $M_*$ . The weight

of the SFS GMM component from the fitting provides an estimate of  $f_{\text{SFS}}^{\text{cen}}$ . In the right panel of Figure 1, we plot the SFS GMM component (blue shaded region) of the  $p(\log \text{SSFR})$  for the SDSS DR7 central galaxies within  $10.6 < \log M_* < 10.8$ . The SFS constitutes  $f_{\text{SFS}}^{\text{cen}} = 0.21$  of the SDSS central galaxies in this stellar mass bin.

Rather than using the  $f_{\text{SFS}}^{\text{cen}}$  values directly, for selecting SF galaxies, we fit  $f_{\text{SFS}}^{\text{cen}}$  as a linear function of  $\log M_*$  similar to [Wetzel et al. \(2013\)](#); [Hahn et al. \(2017a\)](#). We derive the following best-fit:

$$f_{\text{SFS,bestfit}}^{\text{cen}}(M_*) = -0.627 (\log M_* - 10.5) + 0.354. \quad (1)$$

We note that this  $f_{\text{SFS,bestfit}}^{\text{cen}}(M_*)$  is in good agreement with the  $f_{\text{Q}}^{\text{cen}}(M_*; z \sim 0)$  fit from ?. For each central galaxy in our simulation, we assign a probability of it being on the SFS, using Eq. 1 with  $M_*$  at  $z \sim 0$  assigned through SHAM. Based on these probabilities, we randomly identify centrals from our simulation as SF at  $z \sim 0$ . In our model, we make the assumption that once a SF galaxy quenches its star formation, it remains quiescent. Without any quiescent galaxies rejuvenating their star formation, galaxies on the SFS at  $z \sim 0$  are also on the SFS at  $z > 0$ . Using this assumption the SF centrals we select at  $z \sim 0$  are also on the SFS at the initial redshift of our model:  $z \sim 1$ .

Next, we can initialize the SF centrals at  $z \sim 1$  using SHAM  $M_*$ s and assign their initial SFRs based on the observed SFR- $M_*$  relation of the SFS. Observations in the literature at these redshifts, however, not only use galaxy properties derived differently from the SDSS VAGC but they also find SFS with significant discrepancies from one another. [Speagle et al. \(2014\)](#) compiles the SFR- $M_*$  relation of the SFS from 25 studies in the literature, each with different methods of deriving galaxy properties. Even *after* their calibration, for a fixed  $M_* = 10^{10.5} M_\odot$ , the SFRs of the SFSs at  $z \sim 1$  vary by more than a factor of 2 (see Figure 2 of [Speagle et al. 2014](#)). With little consensus on the SFS at  $z \sim 1$ , and consequently its redshift evolution, we flexibly parameterize the SFS SFR ( $\log \text{SFR}_{\text{MS}}(M_*, z)$ ) with free parameters  $m_{M_*}$  and  $m_z$  that characterize the stellar mass and redshift dependences respectively. We parameterize the mean log SFR of the SFS as,

$$\log \overline{\text{SFR}}_{\text{SFS}}(M_*, z) = m_{M_*} * (\log M_* - 10.5) + m_z * (z - 0.05) - 0.11. \quad (2)$$

We assign SFRs to our SF centrals at  $z \sim 1$  by sampling a log-normal distribution centered about  $\log \overline{\text{SFR}}_{\text{MS}}(M_*, z = 1)$  with a constant scatter of 0.3 dex, motivated from observations ([Daddi et al. 2007](#); [Noeske et al. 2007](#); [Magdis et al. 2012](#); [Whitaker et al. 2012](#)). Later in our analysis, for the priors of our parameters  $m_{M_*}$  and  $m_z$ , we conservatively choose a range that encompass the best-fit SFS from [Speagle et al. \(2014\)](#) and measurements from [Moustakas et al. \(2013\)](#) and [Lee et al. \(2015\)](#). With our SF centrals initialized at  $z \sim 1$ , next, we describe how we evolve their SFR and  $M_*$ .

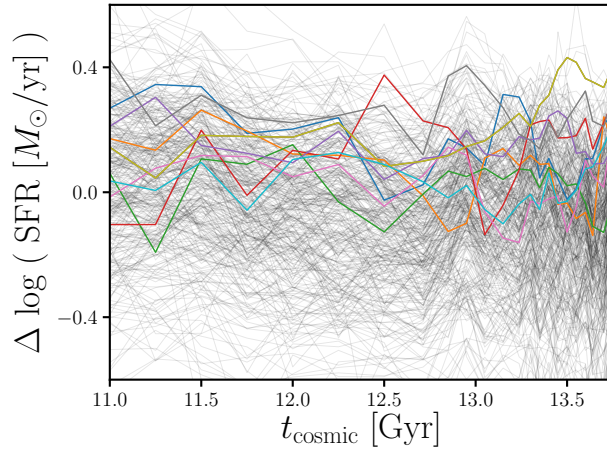


Fig. 2.— Star formation rate with respect to the  $\log \overline{\text{SFR}}_{\text{SFS}} - \Delta \log \text{SFR}$ —as a function of cosmic time for star-forming galaxies in the Illustris simulation. These galaxies have stellar masses within the range  $10^{10.5} - 10^{10.6} M_{\odot}$  at  $z \sim 0$ .  $\log \overline{\text{SFR}}_{\text{SFS}}$  is fit using the Hahn et al. (in prep.) SFS fitting method, the same method we use for our SDSS centrals in Section 3.1. As the  $\Delta \log \text{SFR}(t)$ s in color emphasize how the SFRs of Illustris star-forming galaxies fluctuate about the mean SFS. *The SFR variability in the SFHs of SF centrals in our model (see Section 3.2) is motivated by this  $\Delta \log \text{SFR}(t)$  behavior in Illustris.*

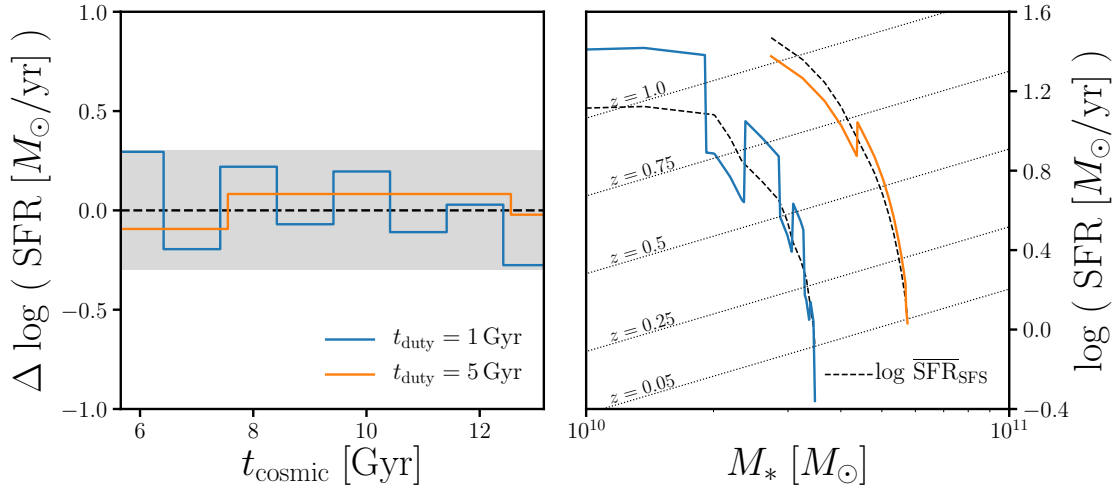


Fig. 3.— *Left:* The  $\Delta \log \text{SFR}$  evolution of two SF centrals using the fiducial model that incorporates star formation variability through a “star formation duty cycle” on two timescales  $t_{\text{duty}} = 1 \text{ Gyr}$  (blue) and  $5 \text{ Gyr}$  (orange).  $\Delta \log \text{SFR}(t)$ s determine the SFHs (Eq. 3), hence it also determines the  $M_*$  growth of the SF central galaxies in our model (Eq. 4). *Right:* The  $\text{SFR}_i$  and  $M_{*,i}$  evolutions of the same two SF central galaxies in our fiducial model with  $t_{\text{duty}} = 1 \text{ Gyr}$  (blue) and  $5 \text{ Gyr}$  (orange). For reference we plot  $\log \overline{\text{SFR}}_{\text{SFS}}(M_{*,i}(t), t)$  for each galaxy (black dashed) and  $\log \overline{\text{SFR}}_{\text{SFS}}(M_*)$  at various redshifts between  $z = 1$  to  $0.05$  (dotted lines). As the  $\text{SFR}_i$  and  $M_{*,i}$  evolutions illustrate, *the SF centrals in our model evolve as their SFRs fluctuate about the SFS.*



### 3.2. Evolving along the Star Formation Sequence

The tight correlation between the SFRs and stellar masses of SF galaxies (the so-called SFS) has been observed to span over four orders of magnitude in stellar mass and extends beyond the local universe out to  $z > 2$  (*e.g.* Noeske et al. 2007; Daddi et al. 2007; ?; Salim et al. 2007; Santini et al. 2009; Karim et al. 2011; Whitaker et al. 2012; Moustakas et al. 2013; Lee et al. 2015; see also references in Speagle et al. 2014). Even in hydrodynamic simulations and semi-analytic models, we find well defined SFSs (see Hahn et al. (in prep.) and references therein). The SFRs of galaxies on the SFS, for a given stellar mass follow a log-normal distribution with a roughly constant scatter ( $\sim 0.3$  dex in observations). Given its persistence in the local Universe, the SFS provides an anchoring relationship to characterize the SFRs and  $M_*$ s of SF galaxies throughout  $z < 1$ . More specifically, *we can characterize the star formation histories (SFHs) of our SF centrals with respect to the mean log SFR of the SFS* (Eq. 2):

$$\log \text{SFR}(M_*, t) = \log \overline{\text{SFR}}_{\text{MS}}(M_*, t) + \Delta \log \text{SFR}(t). \quad (3)$$

Since SFHs determine the  $M_*$  growth of galaxies,  $\Delta \log \text{SFR}$ s in our model dictate the SFHs and  $M_*$  evolution of SF centrals. Below, we describe the prescription for our fiducial  $\Delta \log \text{SFR}(t)$ .

One naive example for  $\Delta \log \text{SFR}(t)$  would be to keep  $\Delta \log \text{SFR}$  fixed from the initial offsets from the  $\log \overline{\text{SFR}}_{\text{SFS}}$  in the initial SFRs of our SF central galaxies at  $z \sim 1$ . SF centrals with higher than average initial SFRs continue evolving above the average SFS, while SF centrals with lower than average initial SFRs continue evolving below the average SFS. In addition to the fact that such a SFH cannot reproduce observations, which we later demonstrate, we do not find such a SFH in SF galaxies of hydrodynamic simulations such as Illustris Vogelsberger et al. (2014); Genel et al. (2014). In Figure 2, we plot  $\Delta \log \text{SFR}$ s of SF galaxies in Illustris as a function of cosmic time. These galaxies have stellar masses within  $10^{10.5} - 10^{10.6} M_\odot$  at  $z = 0$ . At each simulation output, we derive  $\log \overline{\text{SFR}}_{\text{SFS}}$  using the same Hahn et al. (in prep.) fitting method as in Section 3.1 and use it to calculate  $\Delta \log \text{SFR}$  (Eq. 3). As the  $\Delta \log \text{SFR}$ s highlighted in color illustrate, the  $\Delta \log \text{SFR}(t)$ s of SF galaxies do not remain constant, but rather vary about the SFS.

Motivated by the  $\Delta \log \text{SFR}(t)$  of Illustris galaxies, we introduce variability in the SFHs of our SF centrals in the form of a “*star formation duty cycle*”. We parameterize  $\Delta \log \text{SFR}$  to fluctuate about the mean SFS on some duty cycle timescale  $t_{\text{duty}}$  with amplitude randomly sampled from a log-normal distribution with 0.3 dex scatter at every  $t_{\text{duty}}$  timestep. The full SFH of the SF centrals follow Eq. 3. In the left panel of Figure 3, we present  $\Delta \log \text{SFR}(t)$  of SF centrals with our fiducial star formation duty cycle prescription. The two  $\Delta \log \text{SFR}(t)$ s have  $t_{\text{duty}} = 1$  Gyr (blue) and 5 Gyr (orange). The shaded region represents the observed 0.3 dex  $1\sigma$  scatter of the SFS SFR. Although, we do not expect such a simplified model to reflect the exact individual SFHs of SF centrals, for the SF population it captures the

stochasticity from gas accretion, star-bursts, and feedback mechanisms. Furthermore, it allows us to measure the timescale of such variabilities. Also this  $\Delta \log$  SFR prescription by construction reproduces the observed log-normal SFR distribution of the SFS at any point in the model.

Next using our  $\Delta \log$  SFR prescription, we now evolve both the SFR and  $M_*$  of our SF centrals along the SFS. Based on Eq. 3, the SFRs of our SF centrals are functions of  $M_*$ . Meanwhile,  $M_*$  is the integral of the SFR over time:

$$M_*(t) = f_{\text{retain}} \int_{t_0}^t \text{SFR}(M_*, t) dt + M_0. \quad (4)$$

$t_0$  and  $M_0$  are the initial cosmic time and stellar mass at  $z \sim 1$ , respectively.  $f_{\text{retain}}$  here is the fraction of stellar mass that is retained after supernovae and stellar winds; we use  $f_{\text{retain}} = 0.6$  (Wetzel et al. 2013). By solving the differential equation from combining Eqs. 3 and 4, we evolve the SFR and  $M_*$  of our SF centrals. The right panel of Figure 3 presents the  $\text{SFR}_i$  and  $M_{*,i}$  evolutions for the two SF centrals with different  $t_{\text{duty}}$  timescales in the left panel. For reference, we include  $\log \overline{\text{SFR}}_{\text{SFS}}(M_{*,i}(t), t)$  (black dashed) and  $\log \overline{\text{SFR}}_{\text{SFS}}(M_*)$  (dotted lines) at various redshifts between  $z = 1$  to 0.05. As Figure 3 illustrates, using our  $\Delta \log$  SFR prescription the SF centrals evolve as their SFRs fluctuate along the SFS throughout the timesteps of our model.

We continue to evolve our SF central galaxies until the final  $z = 0.05$  snapshot. For the SF centrals in our model, not only do we have SFRs and  $M_*$ s that we evolved but we also have their host halo properties from the **TreePM**  $N$ -body simulation. Using these properties, we can compare our model to observations and constrain the free parameters using observables such as the quiescent fraction and SMF. Once we have a model that reproduces the standard observables we can use the host halo properties to examine observables such as the SHMR. Next, we present this comparison between our model and observations and present the constraints we derive on the role and timescale of star formation variability in the evolution of SF galaxies.

## 4. Results

Our model takes **TreePM** central subhalos and tracks their  $\text{SFR}$  and  $M_*$  evolution using a flexible parameterization of the SFS and SFHs that incorporate variability through a star formation duty cycle. At  $z = 0.05$ , its final timestep, our model provides properties such as the SFR,  $M_*$ , and host halo mass,  $M_h$ , of central galaxies it classifies as SF. We now use these resulting properties to compare our model to observations and constrain its free parameters—the parameters of the Eq. 2 SFS. Since the focus of our model and this paper is on SF centrals, the main observable we use is the SMF of SF SDSS centrals, which we

estimate as

$$\Phi_{\text{SF, cen}}^{\text{SDSS}} = f_{\text{SFS}}^{\text{cen}} \times f_{\text{cen}} \times \Phi^{\text{Li\&White(2009)}}. \quad (5)$$

$f_{\text{SFS}}^{\text{cen}}$  is the fraction of central galaxies on the SFS, which we fit in Eq. 1.  $f_{\text{cen}}$  is the central galaxy fraction from Wetzel et al. (2013) and  $\Phi^{\text{Li\&White(2009)}}$  is the SMF of the SDSS from Li & White (2009). If our model reproduces the observed  $\Phi_{\text{SF, cen}}^{\text{SDSS}}$ , by construction, it also reproduces the observed quiescent fraction.

For the actual comparison of our model to observation, we use the parameter estimation framework of Approximate Bayesian Computation (ABC). ABC has the advantage over standard approaches to parameter inference in that it does not require evaluating the likelihood. It relies only on a simulation of the observed data and a distance metric to quantify the “closeness” between the observed data and simulation. Many variations of ABC has been used in astronomy and cosmology (*e.g.* ???Alsing et al. 2018). We use ABC in conjunction with the efficient Population Monte Carlo (PMC) importance sampling as in (?Hahn et al. 2017a). For initial range of our ABC particles, *i.e.* the priors of our Eq. 2 SFS parameters  $A_z$  and  $m_z$ , we use uniform distributions spanning the ranges **numbers** and **numbers**, respectively. As we mentioned in Section 3.1, the range of the prior were conservatively chosen to encompass the best-fit SFS from Speagle et al. (2014) and measurements from Moustakas et al. (2013) and Lee et al. (2015) at  $z \sim 1$ . Finally, for our distance metric, we formulate a distance between the SMF of the SF centrals in our model to the observed  $\Phi_{\text{SF, cen}}^{\text{SDSS}}$  (Eq. 5):

$$\rho_{\Phi} = \sum_M \left( \frac{\Phi^{\text{sim}} - \Phi_{\text{SF, cen}}^{\text{SDSS}}}{\sigma'_{\Phi}} \right)^2. \quad (6)$$

$\Phi^{\text{sim}}(M)$  is the SMF of the SF centrals in our model and  $\sigma'_{\Phi}(M)$  **is the SMF uncertainty derived using mock catalogs from Li & White (2009)**. For the rest of our ABC-PMC implementation, we strictly follow the implementation of Hahn et al. (2017b) and ?. We refer reader to those papers for further details.

In Figure 6, we present the SMFs (left), SFSs (middle), and  $\sigma_{\log M_*}(\log M_{\text{halo}})$  (right) of two models with different SFH prescriptions run using their respective ABC posterior distributions. One model has **no star formation duty cycle** (red) while the other has a duty cycle of  $t_{\text{duty}} = 1 \text{ Gyr}$  (blue). For both ABC posteriors, the models successfully reproduce  $\Phi_{\text{SF, cen}}^{\text{SDSS}}$ , the SDSS SF central SMF (left). They also have similar SFSs (middle). Despite the similarity in the SFRs and  $M_*$ s, *depending on the timescale of the star formation duty cycle, the models produce significantly different scatter in  $\log M_*$  for a given  $\log M_{\text{halo}}$  — i.e. scatter in the SHMR* (right). Measurements of the scatter in SHMR of our models can be compared to observational constraints on the SHMR in order to better understand and constrain the SFHs of star forming galaxies.

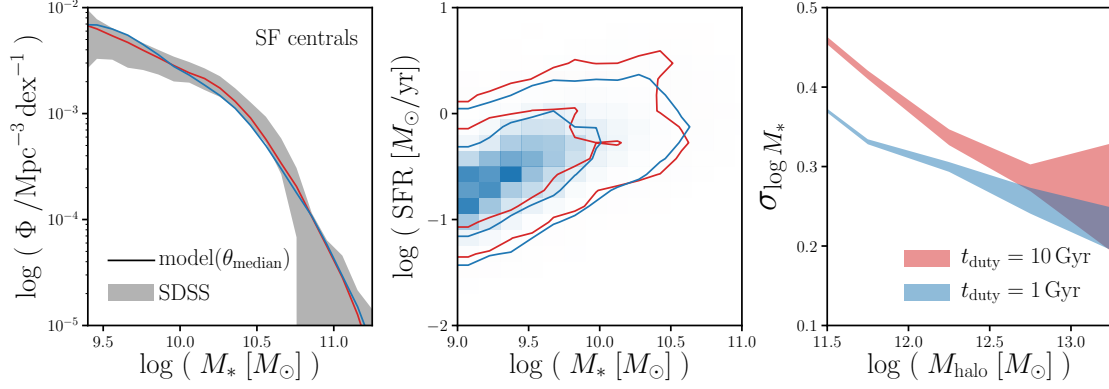


Fig. 4.— The observables of two models with different SFH prescriptions run using their respective ABC posterior distributions. One model has **no star formation duty cycle** (red) while the other has a duty cycle of  $t_{\text{duty}} = 1$  Gyr (blue).

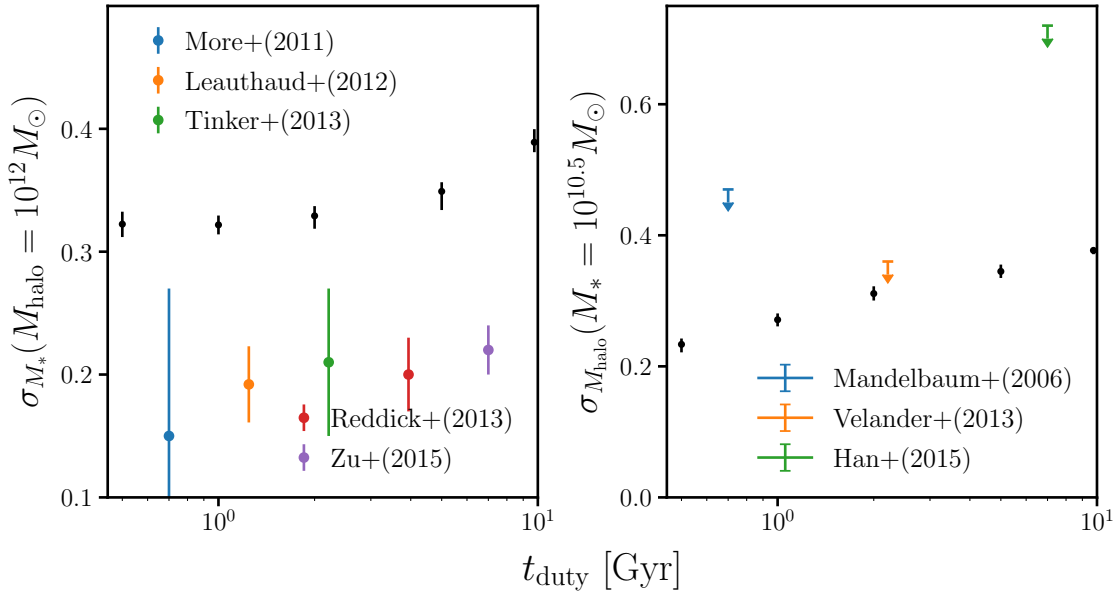


Fig. 5.—

#### 4.1. The Star Formation Duty Cycle

In the previous section we describe our model constructed from blah with different prescriptions for the star formation histories of star-forming galaxies. As the right panel of Figure 6 demonstrates, different prescriptions for the star-forming galaxy star formation predicts different  $\sigma_{\log M_*}$

- Explain how the posteriors from ABC ultimately marginalize over the parameters that incorporate the uncertainty in the SFS
- As Figure 6 already demonstrates, different prescriptions lead to different scatter in the SMHMR.
- No duty cycle model obviously ruled out
- In Figure 5 we present the scatter in  $\sigma_{\log M_*}$
- We find that by decreasing the timescale of stochasticity on a simple SFH model that traces the overall SFS evolution does in fact decrease the scatter seen in the SMHMR. However, even with timescales less than XXXX, we cannot reproduce observations. Ultimately to reproduce observations, we need to add in assembly bias.

Figure 5

#### 4.2. The need for a galaxy assembly bias

- discuss how  $t_{duty}$  is not enough to be consistent with  $\sigma_{M_*}$ .
- first clarify what you mean by galaxy assembly bias
- discuss implementation of galaxy assembly bias
- Figure (pedagogical) of  $d\log SFR$  versus  $dM_h/dt$  for different correlation amounts
- Figure of different  $t_{delay}$  and  $dt_{bias}$
- Figure of  $\sigma_{M_*}$  as a function of duty cycle and realistic  $dt_{bias}$  and  $t_{delay}$

### 5. Discussion

#### 5.1. Rethinking the Main Sequence?

- Test the SMHMR for Louis’s SFHs

## 6. Summary

### A. $z \sim 1$ observations

Much of the results presented in this paper are based on comparison between our model and observations at  $z \sim 0.$ . Our model is initialized at  $z \sim 1$ . Therefore, in this section we test some of the choices we make in our initializations.

- Test impact of  $z \sim 1$  SMF
- Test impact of  $z \sim 1$   $\sigma_{\log M_*}$

## Acknowledgements

It’s a pleasure to thank Louis Abramson, Shy Genel, **more acknowledgements** for valueable discussions.

## REFERENCES

- Abazajian, K. N., Adelman-McCarthy, J. K., Agüeros, M. A., et al. 2009, [The Astrophysical Journal Supplement Series](#), 182, 543
- Alsing, J., Wandelt, B., & Feeney, S. 2018, arXiv:1801.01497 [astro-ph], [arXiv:1801.01497 \[astro-ph\]](#)
- Baldry, I. K., Balogh, M. L., Bower, R. G., et al. 2006, [Monthly Notices of the Royal Astronomical Society](#), 373, 469
- Blanton, M. R., & Moustakas, J. 2009, [Annual Review of Astronomy and Astrophysics](#), 47, 159
- Blanton, M. R., & Roweis, S. 2007, [The Astronomical Journal](#), 133, 734
- Blanton, M. R., Schlegel, D. J., Strauss, M. A., et al. 2005, [The Astronomical Journal](#), 129, 2562
- Brinchmann, J., Charlot, S., White, S. D. M., et al. 2004, [Monthly Notices of the Royal Astronomical Society](#), 351, 1151
- Campbell, D., van den Bosch, F. C., Hearin, A., et al. 2015, [Monthly Notices of the Royal Astronomical Society](#), 452, 444
- Chabrier, G. 2003, [Publications of the Astronomical Society of the Pacific](#), 115, 763
- Conroy, C., Wechsler, R. H., & Kravtsov, A. V. 2006, [The Astrophysical Journal](#), 647, 201
- Daddi, E., Dickinson, M., Morrison, G., et al. 2007, [The Astrophysical Journal](#), 670, 156
- Davis, M., Efstathiou, G., Frenk, C. S., & White, S. D. M. 1985, [The Astrophysical Journal](#), 292, 371
- Drory, N., Bundy, K., Leauthaud, A., et al. 2009, [The Astrophysical Journal](#), 707, 1595

- Genel, S., Vogelsberger, M., Springel, V., et al. 2014, [Monthly Notices of the Royal Astronomical Society](#), 445, 175
- Hahn, C., Tinker, J. L., & Wetzel, A. R. 2017a, [The Astrophysical Journal](#), 841, 6
- Hahn, C., Vakili, M., Walsh, K., et al. 2017b, [Monthly Notices of the Royal Astronomical Society](#), 469, 2791
- Hahn, C., Blanton, M. R., Moustakas, J., et al. 2015, [The Astrophysical Journal](#), 806, 162
- Ilbert, O., McCracken, H. J., Le Fèvre, O., et al. 2013, [Astronomy and Astrophysics](#), 556, A55
- Karim, A., Schinnerer, E., Martínez-Sansigre, A., et al. 2011, [The Astrophysical Journal](#), 730, 61
- Lee, N., Sanders, D. B., Casey, C. M., et al. 2015, [The Astrophysical Journal](#), 801, 80
- Leja, J., van Dokkum, P., & Franx, M. 2013, [The Astrophysical Journal](#), 766
- Li, C., & White, S. D. M. 2009, [Monthly Notices of the Royal Astronomical Society](#), 398, 2177
- Magdis, G. E., Daddi, E., Béthermin, M., et al. 2012, [The Astrophysical Journal](#), 760, 6
- Mamon, G. A., Sanchis, T., Salvador-Solé, E., & Solanes, J. M. 2004, [Astronomy and Astrophysics](#), 414, 445
- Marchesini, D., van Dokkum, P. G., Förster Schreiber, N. M., et al. 2009, [The Astrophysical Journal](#), 701, 1765
- Moustakas, J., Coil, A. L., Aird, J., et al. 2013, [The Astrophysical Journal](#), 767, 50
- Muzzin, A., Marchesini, D., Stefanon, M., et al. 2013, [The Astrophysical Journal](#), 777, 18
- Noeske, K. G., Weiner, B. J., Faber, S. M., et al. 2007, [The Astrophysical Journal Letters](#), 660, L43
- Peng, Y.-j., Lilly, S. J., Kovač, K., et al. 2010, [The Astrophysical Journal](#), 721, 193
- Salim, S., Rich, R. M., Charlot, S., et al. 2007, [The Astrophysical Journal Supplement Series](#), 173, 267
- Santini, P., Fontana, A., Grazian, A., et al. 2009, [Astronomy and Astrophysics](#), 504, 751
- Speagle, J. S., Steinhardt, C. L., Capak, P. L., & Silverman, J. D. 2014, [The Astrophysical Journal Supplement Series](#), 214, 15
- Tinker, J., Wetzel, A., & Conroy, C. 2011, ArXiv e-prints, 1107, arXiv:1107.5046
- Tinker, J. L., Hahn, C., Mao, Y.-Y., & Wetzel, A. R. 2017, arXiv:1705.08458 [astro-ph], [arXiv:1705.08458 \[astro-ph\]](#)
- Vale, A., & Ostriker, J. P. 2006, [Monthly Notices of the Royal Astronomical Society](#), 371, 1173
- Vogelsberger, M., Genel, S., Springel, V., et al. 2014, [Monthly Notices of the Royal Astronomical Society](#), 444, 1518
- Wetzel, A. R., Cohn, J. D., & White, M. 2009, [Monthly Notices of the Royal Astronomical Society](#), 395, 1376

- Wetzel, A. R., Tinker, J. L., & Conroy, C. 2012, [Monthly Notices of the Royal Astronomical Society](#), 424, 232
- Wetzel, A. R., Tinker, J. L., Conroy, C., & van den Bosch, F. C. 2013, [Monthly Notices of the Royal Astronomical Society](#), 432, 336
- . 2014, [Monthly Notices of the Royal Astronomical Society](#), 439, 2687
- Wetzel, A. R., & White, M. 2010, [Monthly Notices of the Royal Astronomical Society](#), 403, 1072
- Whitaker, K. E., van Dokkum, P. G., Brammer, G., & Franx, M. 2012, [The Astrophysical Journal Letters](#), 754, L29
- White, M. 2002, [The Astrophysical Journal Supplement Series](#), 143, 241
- White, M., Cohn, J. D., & Smit, R. 2010, [Monthly Notices of the Royal Astronomical Society](#), 408, 1818
- Yang, X., Mo, H. J., & van den Bosch, F. C. 2009, [The Astrophysical Journal](#), 695, 900
- Yang, X., Mo, H. J., van den Bosch, F. C., & Jing, Y. P. 2005, [Monthly Notices of the Royal Astronomical Society](#), 356, 1293



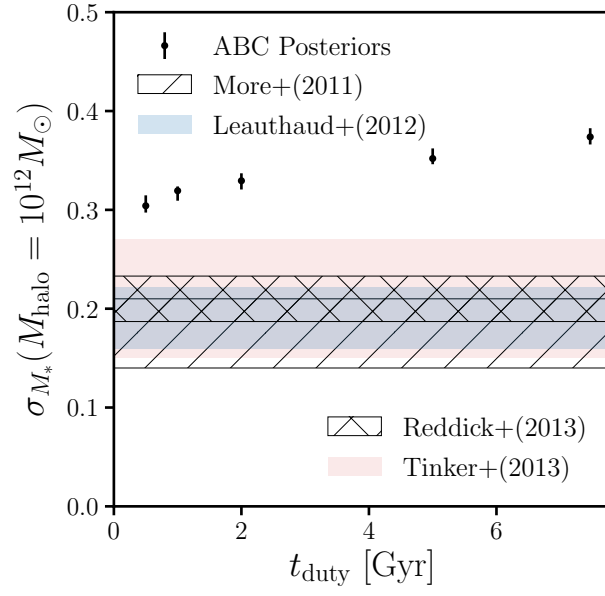


Fig. 6.—